International Journal of Pharmaceutics 366 (2009) 124–132

Contents lists available at ScienceDirect

International Journal of Pharmaceutics

journal homepage: www.elsevier.com/locate/ijpharm

Particulate drug interactions with polymeric and elastomeric valve components in suspension formulations for metered dose inhalers

Jeff James [a,*], Martyn Davies [a], Richard Toon [b], Phil Jinks [b], Clive J. Roberts [a]

[a] Laboratory of Biophysics and Surface Analysis, School of Pharmacy, The University of Nottingham, Nottingham, NG7 2RD, UK
[b] 3M Drug Delivery Ltd., 1 Morley Street, Loughborough, Leicestershire, LE11 1EP, UK

ARTICLE INFO

Article history:
Received 23 June 2008
Received in revised form 21 August 2008
Accepted 4 September 2008
Available online 20 September 2008

Keywords:
Pressurised metered dose inhalers (pMDIs)
Atomic force microscopy (AFM)
Surface energy
Surface component analysis (SCA)

ABSTRACT

Purpose: To characterise the adhesive interactions between three pulmonary active pharmaceutical ingredient (API) materials and the components of pressurised metered dose inhalers (pMDIs) obtained from two commercially available products (termed 'Prod-1' and 'Prod-2'). This is of potential interest, as a greater understanding of the interactions between specific APIs and surfaces may aid manufacturers in component selection during pMDI system development.
Methods: The theoretical work of adhesion (ΔG_{132}) for each API–pMDI component interaction was calculated using the surface component analysis (SCA) approach. These results were correlated with corresponding API–pMDI component separation energy measurements determined using colloid probe AFM.
Results: Strong correlations existed between separation energy and the ΔG_{132} parameters where the polar contribution was accounted for. This highlighted the adhesive influence of polar surface energy on each interaction in this study. Generally the largest adhesive interactions involved APIs and pMDI components which have a bipolar surface energy (i.e. both γ^- and $\gamma^+ > 1\,mJ\,m^{-2}$).
Conclusions: For each API–pMDI interaction in this study, the polar component of surface energy has the greater influence on adhesive events. The bipolar surface energetics of certain APIs and pMDI components were deemed responsible for the increased adhesive interactions observed with these materials. This study highlights that different materials can have different effects on the adhesive interactions with particulate APIs; information that could aid the manufacturer in producing more effective and efficient pMDI systems.

1. Introduction

Suspension pressurised metered dose inhalers (pMDIs) generally consist of particulate active pharmaceutical ingredients (APIs) suspended in a hydrofluoroalkane (HFA) propellant within an aluminium canister, usually in the presence of one or more excipients. A cross section of a typical pMDI valve is shown in Fig. 1. After initial actuation of the unit, a metered dose of the formulation is constantly present within the metering chamber of the valve and replaced with fresh formulation after each subsequent actuation. Therefore, a dose of the particulate formulation is in constant contact with the components of the valve (metering chamber, stem, seals and spring) until exhaustion of the unit occurs. Clearly then, the physical stability of particulate formulations in the pMDI valves is pertinent in terms of dose uniformity and, potentially, regulatory compliance. It has been previously demonstrated that pMDI device components used with propellants (chlorofluorocarbon or hydrofluoroalkane) can result in inefficient device performance, due to adhesion of the suspended particulate API material to the interior of pMDI device surfaces (Vervaet and Byron, 1999). Other consequences of device–propellant interactions include adsorption, poor lubrication and elastomer swelling (Vervaet and Byron, 1999). Consequently, there have been attempts to counter these phenomena, such as coating the canister with various polymers to reduce adhesion (Traini et al., 2006), the development of low swell elastomers such as ethylene propylene diene monomer (EPDM) and the use of various surfactants within the pMDI formulation. In the case considering suspension pMDI formulations, adhesion to pMDI surfaces can also potentially occur (Young et al., 2003).

Atomic force microscopy (AFM) has, in recent years, been employed to gain some insight into drug particle interactions within model pMDI systems (e.g., Ashayer et al., 2004; Traini et al., 2005; James et al., 2007). Most assessments have been semi-quantitative and non-empirical (Chibowski et al., 1992). More recently, there have been attempts to relate the thermodynamic

* Corresponding author.
E-mail addresses: paxjj@nottingham.ac.uk (J. James), rtoon@mmm.com (R. Toon), clive.roberts@nottingham.ac.uk (C.J. Roberts).

0378-5173/$ – see front matter © 2008 Elsevier B.V. All rights reserved.
doi:10.1016/j.ijpharm.2008.09.018

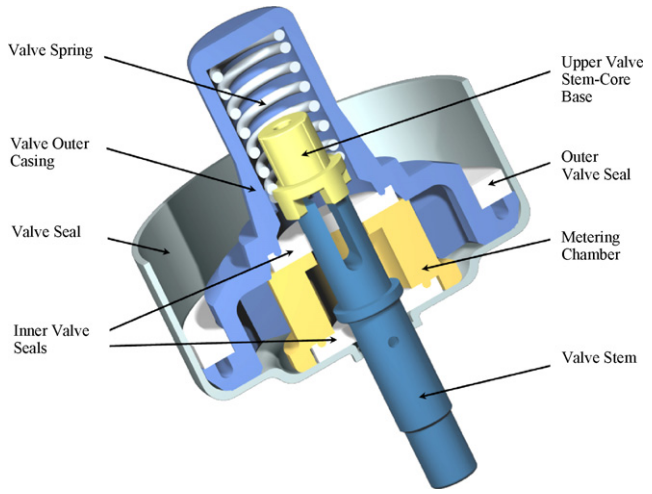

Fig. 1. Diagram illustrating a cross section of a pMDI valve.

work of adhesion of various API materials to the surface energy of polymer-coated and non-coated metallic pMDI canisters (Traini et al., 2006). However, to the authors' knowledge, there has been little assessment of the interactions between particulate APIs and both the elastomeric and polymeric valve components of a pMDI system. This is somewhat surprising as some commercially available products use both polymeric and elastomeric components within their valves. One could assume that the assessment of particle–component interactions in the metering chamber of a pMDI system would be of considerable interest when considering the variety of materials employed and the potential physical changes that may occur during the storage of suspension formulations.

This study primarily compares the adhesive interactions of pMDI valve components from two different commercially available products, to selected API materials in the presence of the model propellant, 2H, 3H decafluoropentane (mHFA). In addition, this study also determines the surface energy of each API and pMDI valve component using contact angle (CA) measurements. Subsequently the theoretical adhesive forces were calculated from the CA measurements using the surface component analysis (SCA) approach (Traini et al., 2005). The theoretical work of adhesion values were correlated with those determined experimentally using the AFM colloid probe technique (Davies et al., 2005).

1.1. The surface component analysis (SCA) principle

The SCA method for determining the work of adhesion from contact angle measurements was first devised by van Oss (van Oss et al., 1988) and is essentially based on an adaptation of the DLVO theory (Derjaguin and Landau, 1941; Verwey and Overbeek, 1948). The theory behind the SCA principle is extensive and can be found in the literature (van Oss et al., 1988; van Oss, 1994), whereas only a brief overview of the background and key points will be given here.

DLVO theory is based on the assumption that London van der Waals forces and electrostatic forces (primarily repulsive) dictate intermolecular and interparticulate interactions in a liquid environment. This has not been validated in non-aqueous pMDI formulations (Vervaet and Byron, 1999; Smyth, 2003) since in such cases interactions are dictated by a combination of London van der Waals forces, electrostatic double-layer interactions and Lewis acid/base interactions (van Oss, 1993; van Oss and Busscher, 1997). Moreover, it was predicted that London van der Waals forces and Lewis acid/base interactions would dominate these interactions, since the diffuse nature of the electric double-layers in these systems would result in negligible electrostatic repulsive forces (Pugh et al., 1983). Therefore, the SCA model focuses on the Lifshitz van der Waals and Lewis acid/base interactions. The Lifshitz van der Waals interactions are apolar in nature and consist of a combination of the dispersive, induction and orientation components of van der Waals interactions. The Lewis acid/base interactions are polar in nature. The surface energy of any interaction is a combination of the dispersive Lifshitz van der Waals (γ^{LW}) contribution and the Lewis acid/base (γ^{AB}) contribution.

Subsequently, adopting the Good–Girifalco–Fowkes combination rule (Good and Girifalco, 1960; Fowkes, 1963), the interfacial energy parameters between dissimilar substances (1 and 2) within an apolar medium (3, where the polar γ contributions (γ^+ and γ^-) both equal 0), the free energy of an interaction can be stated in the following equation:

$$\Delta G_{132} = 2\left(\sqrt{\gamma_1^{LW}\gamma_3^{LW}} + \sqrt{\gamma_2^{LW}\gamma_3^{LW}} - \sqrt{\gamma_1^{LW}\gamma_2^{LW}} - \gamma_3^{LW} - \sqrt{\gamma_1^{+}\gamma_2^{-}} - \sqrt{\gamma_1^{-}\gamma_2^{+}}\right) \quad (1)$$

(Note: the full explanation and derivation of this equation is detailed in Traini et al., 2005, referenced in the appropriate section of this article.)

Thus, the free energy of interaction for the dispersive and polar forces can be calculated if the user has a knowledge of the dispersive and polar surface energies of each solid (1 and 2) and the liquid media (3).

1.2. Direct surface energy measurements using AFM

Since the interfacial free energy of interaction (ΔG_{132}) is equal to the work of adhesion (W_{adh}), comparisons can be made between ΔG_{132} determined by the SCA model, and W_{adh} measurements directly determined by colloid probe AFM force measurements, via one of the contact models; the Johnson–Kendall–Roberts model (JKR – Eq. (2)) or the Derjaguin–Müller–Toporov model (DMT – Eq. (3)).

$$\text{JKR model}: F_{ad} = \frac{3}{2}\pi R^* W_{adh} \quad (2)$$

$$\text{DMT model}: F_{adh} = 2\pi R^* W_{adh} \quad (3)$$

In both equations, F_{adh} is the measured force of adhesion between two surfaces and R^* is the contact radius of the particle against the surface. The JKR model is usually applied to systems with large particle radii, high surface energies and compliant materials (Johnson et al., 1971; Derjaguin et al., 1975), whereas the DMT model is usually applied to rigid particles with small radii. The use of each model is dependant on the nature of each interactive system.

1.3. Summary of investigative aims

This study investigated the adhesive interactions between three API materials and pMDI valve components from two different products (denoted 'Prod-1' and 'Prod-2'). The surface chemistry of each of these pMDI components was assessed using X-ray photoelectric spectroscopy (XPS). The surface morphology of each component was determined using scanning electron microscopy (SEM). The surface roughness of each component was determined using AFM imaging. Using the SCA approach, the theoretical work of adhesion (ΔG_{132}) was determined for each pMDI valve component and API; these theoretical values were subsequently compared to

direct API–pMDI valve component separation energy interactions determined using the AFM colloid probe technique. This study subsequently investigated any relationships which exist between the surface chemistry of each API/pMDI valve material, and their corresponding adhesive interactions.

2. Materials and methods

2.1. Materials

The polymeric and elastomeric valve components from two separate commercially available products (Prod-1 and Prod-2) were purchased. Each canister was fired to exhaustion. The canisters were then cut open and the valve components were carefully removed. Each valve component was then thoroughly washed several times in ethanol to remove traces of formulation and then dried. Metallic components such as the springs were also evaluated for comparison purposes. Salbutamol sulphate and salmon calcitonin were supplied by Sigma–Aldrich (Gillingham, UK). Mometasone furoate was supplied by Euroasian Chemicals (Mumbai, India). The model propellant 2H, 3H-decafluoropentane (mHFA) was supplied by Apollo Scientific (Derbyshire, UK). The mHFA was 99.7% pure with moisture content of 50 ppm. Fresh samples of mHFA were used for each experiment to negate possible effects of water diffusion, which could have an effect on particle adhesion (Traini et al., 2005). Diiodomethane and ethylene glycol were supplied by Sigma–Aldrich, while deionised water was produced by a pure Elga filter (Elga Lab Water, High Wycombe, UK).

3. Methods

3.1. Scanning electron microscopy (SEM)

The surface morphology of each pMDI component was investigated using the JEOL 6060 LV SEM (JEOL (UK) Ltd., Welwyn Garden City, UK). Each component was mounted onto an adhesive carbon stub and gold-coated (20 nm thickness) prior to analysis. SEM analysis was carried out at an accelerating voltage of 2 kV and a spot size of 62 nm.

3.2. X-ray photoelectric spectroscopy (XPS)

In order to determine their surface elemental composition, each polymeric and elastomeric pMDI valve component underwent XPS analysis using an Axis-Ultra spectrometer (Kratos Analytical, Manchester, UK). The elemental compositions of each material were determined using relative sensitivity factors (empirically modified by the manufacturer) and Casa XPS peak-fitting software. The irradiating X-rays were emitted at a take-off angle of 90°.

3.3. Atomic force microscopy – topographical imaging acquisition

AFM imaging was used in order to determine the root mean square (RMS) roughness of each pMDI valve component. Each sample was imaged using an EnviroScope AFM (Veeco, Santa Barbara, USA) in tapping mode using NPS cantilevers (Veeco). A scan rate of 1.0 Hz was used over a 5 μm × 5 μm scan size. Three images were acquired from each pMDI component surface and the RMS roughness was calculated using software incorporated in the AFM system, via the following equation:

$$R_{\mathrm{rms}} = \sqrt{\frac{1}{n}\sum_{i=1}^{n} y_i^2} \quad (4)$$

where n is the number of points in the topography profile, i is the asperities and y_i is the distance between the asperities.

3.4. Atomic force microscopy – separation energy determination

The interaction between each API and each pMDI component was determined using AFM colloid probe technique. The spring constants of a number of silicon nitride V-shaped cantilevers (Veeco) were determined using the thermal method (Gibson et al., 2003). The spring constants for these cantilevers were between 0.3 and 0.34 N m^{-1}. Using these cantilevers, colloid probes were made using a method described elsewhere (Eve et al., 2002; Davies et al., 2005) but to summarise, single particles of each API were attached to individual cantilevers using an epoxy resin at least 48 h before use. The tip radius of each probe was characterised by tip self-imaging using a previously reported procedure described elsewhere (Hooton et al., 2004) in order to check the integrity of the probe throughout the experiment. Before the required force of adhesion data, it was also important to determine the deflection sensitivity of the cantilever. Therefore, force curves against a freshly cleaned borosilicate glass cover slip were collected. The glass cover slip acted a non-indenting reference surface thus the deflection sensitivity of the cantilever could be accurately determined. The borosilicate glass cover slip was cleaned, rinsed and dried using Piranha solution (a mixture of 30% H_2O_2 and 70% concentrated H_2SO_4 in water (1:4)), deionised water and nitrogen gas respectively. Sixteen deflection sensitivity force curves were collected using an EnviroScope AFM (Veeco) at a distance of 100 nm between sampling points. Following this, 100 force measurements were taken using each colloid probe against each pMDI component surface, in the presence of 20 ml mHFA, using the same EnviroScope AFM (Veeco). A maximum load of 10 nN was applied to push the tips into contact with the sample surfaces. Each test was conducted at 10 °C. In this instance, a distance of 500 nm was employed between sampling points. The deflection sensitivity regime was repeated after the force of adhesion data acquisition in order to verify that the deflection sensitivity had not changed substantially during the experiment. Tip characterisation was also repeated in order to check the integrity of the tip throughout the experiment. Three colloid probes were used for each interaction. The separation energy between each API and each pMDI surface was determined by integrating the area under each force curve produced, using custom built software.

The integrity of the colloid probes was carefully monitored throughout the study, in order to ensure against significant variations in the contact area of the API particle. In addition to the AFM tip characterisation imaging, each probe was imaged using SEM before and after each force experiment. This was done to ensure that no major changes in contact area or particle morphology had occurred during the acquisition of force data. The probes were not gold-coated, as this would render them useless for AFM force data acquisition. Furthermore, following SEM analysis, each colloid probe was scanned with Static Line II (Agar Scientific, Stansted, UK) to remove possible electrostatic charges at least 24 h before they were used for AFM force data acquisition.

3.5. Contact angle measurements

The contact angles of water, diiodomethane and ethylene glycol were determined against each pMDI component, using the sessile drop method (Good, 1993; Buckton et al., 1995; Kwok et al., 1998). Results were obtained using a DSA 100M optical Contact Angle meter (KSV Instruments, Helsinki, Finland) at ambient conditions. Twenty drops of each solvent (~100 pl) were dispensed

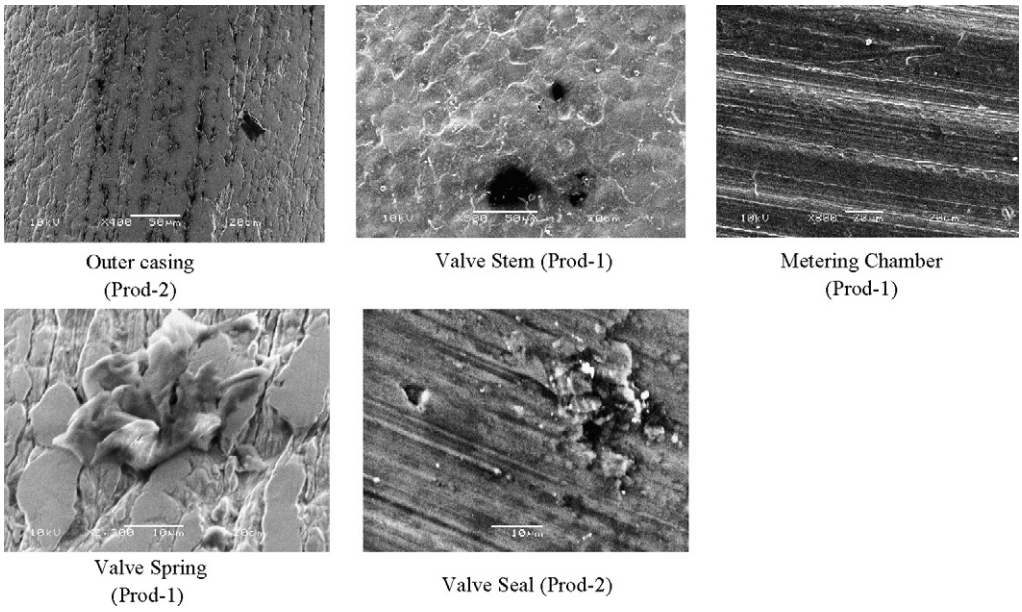

Fig. 2. Example SEM images of various valve component surfaces at micrometre scales.

onto different areas of the surface of each pMDI component. Using the internal high-speed camera, the contact angle of the drop was recorded at 0.01 s intervals and the contact angles observed during this time period were determined by the software incorporated within the system. The contact angles of the three liquids on each API were also determined. Lightly pressed compacts of salbutamol sulphate, mometasone furoate and salmon calcitonin were prepared by manually pressing the sample powders by hand very lightly onto an adhesive carbon stub (Agar Scientific). These samples were mounted by vertically inverting the stub onto a bed of the powder sample; this method was employed to prevent the powder 'rolling' on the adhesive face of the stub, thus avoiding the alteration of the surface to be analysed. The disk formed was approximately 12 mm in diameter and 1 mm thick, and the samples were analysed as prepared. Prior to contact angle analysis, these powder compacts underwent AFM roughness determination in the same manner as the pMDI components (discussed earlier).

On completion, a custom built spreadsheet was used to determine the dispersive and polar surface energy of each material, in accordance with the following equation:

$$(1+\cos\theta)\gamma_L = 2\left(\sqrt{\gamma_S^{LW}\gamma_L^{LW}} + \sqrt{\gamma_S^{+}\gamma_L^{-}} - \sqrt{\gamma_S^{-}\gamma_L^{+}}\right) \quad (5)$$

where γ_L is the surface tension of the test liquid. In addition, $\gamma_S{}^{LW}$ and $\gamma_L{}^{LW}$ are the dispersive Lifshitz component of surface energy for the test solid and test liquid respectively, while $\gamma_S{}^{-}$, $\gamma_S{}^{+}$, $\gamma_L{}^{-}$ and $\gamma_L{}^{+}$ are the polar components of surface energy for the test solid and test liquid respectively.

The theoretical work of adhesion values were also determined using a custom built spreadsheet, in accordance with Eq. (1).

4. Results and discussion

4.1. SEM imaging and AFM roughness analysis

Examples of SEM images of the pMDI component surfaces are shown in Fig. 2. From these images, it can be seen that the surface topographies can vary considerably between different materials. For example, asperities can be seen on the surfaces of the valve seals, while striations are visible on the metering chambers. It can also be observed that the spring has a non-uniform surface. These features could be a result of manufacturing processes such as drawing for the springs and disk-pressing for the seals. The RMS roughness calculations support the SEM data. Table 1 shows the RMS roughness for each of these materials. Both the SEM images and RMS roughness data suggest irregular surface characteristics and prominent asperities for certain materials.

Both the SEM imaging and tip characterisation imaging of the cantilevers functionalised with drug particles, confirmed the integrity of the particles. The drug particles were clearly proud of the cantilever surface and the morphologies of the particles were unchanged throughout the experiment (images not shown).

It is well known that the adhesion of two surfaces can be influenced by the surface roughness of the two contiguous bodies (Buckton, 1995; Katainen et al., 2006). Therefore, it was important to characterise the roughness of each API and pMDI component. While the topographies of each surface could be measured individually, these measurements would only be indicative, since the interacting topographies would differ for each measurement (Hooton et al., 2004). A better indication of whether the surface roughness of each API–pMDI component combination is directly affecting their adhesive interaction is to statistically determine the normality of the force distribution. It has previously been demonstrated that an increase in surface roughness results in a log-normal distribution of adhesion measurements (Price et al., 2002; Young et al., 2004) whereas; normal distributions exist for

Table 1
The RMS roughness of each pMDI component used in this study.

pMDI component/API	Product 1	Product 2
	RMS roughness (nm) (±S.D.)	
Metering chamber	12.8 ± 1.1	9.6 ± 0.7
Valve seal	17.7 ± 0.9	4.9 ± 1.4
Outer casing	13.4 ± 3.7	18.8 ± 5.2
Valve stem	38.4 ± 4.5	16.9 ± 2.7
Valve spring	57.5 ± 4.2	53.3 ± 14.2
Salbutamol sulphate compacts	84.49 (6.99)	
Mometasone furoate compacts	91.37 (7.08)	
Salmon calcitonin compacts	62.10 (4.93)	

Table 2
The elemental composition of each pMDI component used in this study, as determined by XPS.

Manufacturer	pMDI Component	Oxygen 1s (%)	Carbon 1s (%)	Fluorine 1s (%)	Carboxyl group (%)	Hydroxyl group (%)	Iron (%)	Chromium 1s (%)	Nitrogen 1s (%)
Prod-1	Metering chamber	14.4	78.4	4.9	2.9	2.6	–	–	–
	Valve seal	20.0	60.2	–	2.7	3.4	–	–	–
	Outer casing	21.2	72.6	5.3	2.3	4.9	–	–	–
	Valve stem	36.2	60.0	–	28.5	–	–	–	–
	Valve spring	0.2	0.8	–	–	–	85.0	12.6	0.8
Prod-2	Metering chamber	24.5	71.3	3.9	3.1	4.4	–	–	–
	Valve seal	30.0	51.6	–	2.8	4.4	–	–	–
	Outer casing	24.7	71.4	2.2	7.9	10.2	–	–	–
	Valve stem	31.0	61.6	–	23.5	2.7	–	–	–
	Valve spring	0.2	0.5	–	–	–	88.0	10.9	0.1

Table 3a
The theoretical work of adhesion (ΔG_{132}) between Prod-1 pMDI components and each API used in this study.

pMDI component	Salbutamol sulphate			Mometasone furoate			Salmon calcitonin		
	(γ^{LW})	(γ^{AB})	(γ^{TOT})	(γ^{LW})	(γ^{AB})	(γ^{TOT})	(γ^{LW})	(γ^{AB})	(γ^{TOT})
	Product 1; theoretical work of adhesion (mJ m^{-2})								
Metering chamber	14.73	14.78	29.51	15.23	9.60	24.83	14.61	13.67	28.27
Valve seal	14.03	19.50	33.53	14.51	11.69	26.20	13.92	18.16	32.08
Outer casing	16.31	16.14	32.45	16.87	9.49	26.36	16.18	15.06	31.24
Valve stem	18.94	24.25	43.19	19.59	12.66	32.25	18.79	22.84	41.64
Valve spring	13.34	42.48	55.83	13.80	19.20	33.00	13.24	40.43	53.67

smoother, more highly ordered surfaces (Price et al., 2002; Buckton et al., 1995). This was confirmed as frequency distribution histogram plots of the measured separation energies between the API particles, and the metallic and polymeric surfaces gave rise to normal distributions. These results are somewhat expected with polymeric surfaces, which are generally smooth and highly ordered (Fowkes, 1983).

The surface roughness of each API powder compact used for the contact angle experiments could also influence the measured contact angles. While it is still a debatable issue, it is believed that a surface with roughness value of less than 100 nm is not significantly rough enough to influence the measured contact angle (Buckton, 1995). Table 1 indicates that the roughness of each pMDI component sample and API compact is below this value and therefore it is assumed that their surface roughness has not significantly affected the measured contact angles.

4.2. pMDI component surface chemistry analysis by XPS

The elemental and functional-group composition of each pMDI component is detailed in Table 2. There is clearly a high level of surface carbon and oxygen detected in the non-metallic pMDI components, illustrating their polymeric nature. Carboxylic and hydroxyl groups were also detected on the surface of the metering chambers and valve outer casings.

4.3. Surface energy of API materials and components determined by CA measurements

The total surface energy (determined using the CA sessile drop method) for each of the API materials are summarised in Fig. 3a. While there was little difference in the dispersive surface free energies (γ^{LW}) of each API, there were considerable variations in the electron-donor (γ^{-}) and electron-acceptor (γ^{+}) portions of the API surface energetics. When considering the dispersive component of surface energy, the ranking for the API materials is mometasone furoate > salbutamol sulphate > salmon calcitonin. However, when considering the polar components, the rankings are salbutamol sulphate > salmon calcitonin > mometasone furoate for γ^{+} and mometasone furoate > salbutamol sulphate > salmon calcitonin for γ^{-}.

The surface energy results summarised in Fig. 3b and c indicate that there are little differences in dispersive surface energy of each pMDI component. However, the valve components which generally have polymeric surfaces have a lower polar surface energy (γ^{-} in particular) than those of the non-polymeric surfaces, such as the spring. Surfaces which are polymeric in nature typically exhibit low polar surface energy due to their highly ordered symmetrical nature and bond similarity (Fowkes, 1983). Therefore, a lower polar surface energy would be expected for polymeric components compared to that of the metallic components.

Table 3b
The theoretical work of adhesion (ΔG_{132}) between Prod-2 pMDI components and each API used in this study.

pMDI component	Salbutamol sulphate			Mometasone furoate			Salmon calcitonin		
	(γ^{LW})	(γ^{AB})	(γ^{TOT})	(γ^{LW})	(γ^{AB})	(γ^{TOT})	(γ^{LW})	(γ^{AB})	(γ^{TOT})
	Product 2; theoretical work of adhesion (mJ m^{-2})								
Metering chamber	19.34	19.80	39.14	20.00	11.00	31.00	19.18	18.56	37.75
Valve seal	16.59	21.84	38.43	17.15	11.31	28.46	16.45	20.59	37.04
Outer casing	20.20	22.48	42.68	20.89	12.46	33.35	20.04	21.08	41.11
Valve stem	19.52	18.64	38.16	20.19	9.82	30.01	19.37	17.54	36.91
Valve spring	18.35	33.44	51.79	18.98	15.94	34.92	18.21	31.70	49.91

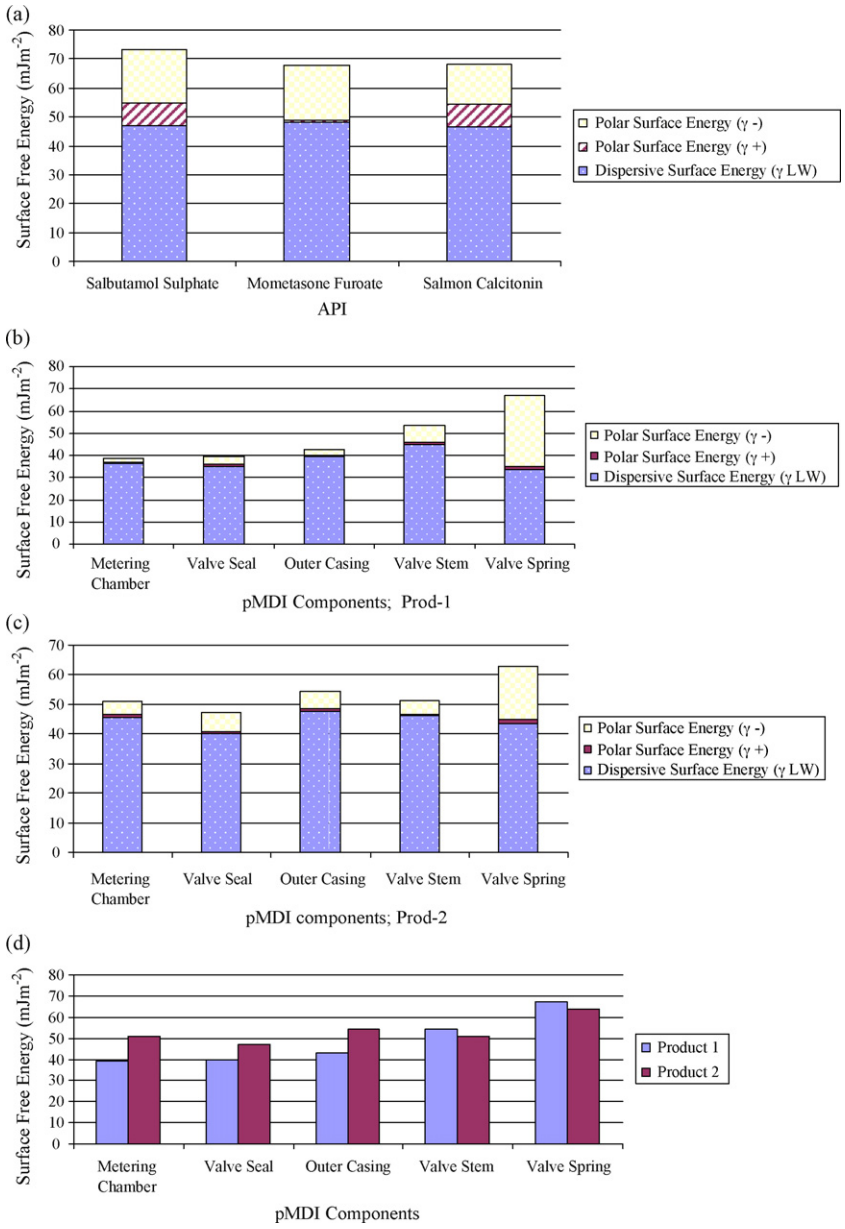

Fig. 3. (a) The surface energies of each API used in this study (determined by CA measurement). The graph illustrates the relative dispersive and polar components of each surface energy result. (b) Surface energies of Prod-1 pMDI valve components (determined by CA measurement). The graph illustrates the relative dispersive and polar components of each surface energy result. (c) Surface energies of Prod-2 pMDI valve components (determined by CA measurement). The graph illustrates the relative dispersive and polar components of each surface energy result. (d) Total surface energies of Prod-1 and Prod-2 pMDI valve components used in this study (determined by CA measurement).

4.4. Calculating the theoretical work of adhesion for each API–pMDI component interaction

The theoretical work of adhesion between each API and each pMDI component can be calculated from the surface energy data obtained using the SCA approach in non-aqueous media (Traini et al., 2005). Tables 3a and 3b show the theoretical work of adhesion between each API and the pMDI components from each product. From the surface tension parameters for mHFA ($\gamma^{LW} = 13.59$, $\gamma^{+} = 0$ and $\gamma^{-} = 0$; Traini et al., 2006), it is understood that mHFA will have no polar contribution to the interactions between each API and pMDI component.

These results indicate the importance of the polar contributions of each material's surface energy. For example, when ranking the dispersive component of theoretical work of adhesion alone, the rank order for Prod-1 components and salbutamol sulphate is: valve stem > bottle emptier > metering chamber > valve seal > valve spring. However, when the polar contribution is included, the rank order of for Prod-1 components and salbutamol sulphate becomes: valve spring > valve stem > valve seal > bottle emptier > metering chamber. Similar trends exist when considering the API–pMDI component interactions for Prod-2. Overall, these differences serve to highlight the significance of the polar contribution of surface energy when considering the adhesive interactions between two materials.

4.5. Separation energies determined using AFM

As stated previously, separation energies between each API and each pMDI component were determined using AFM by integrating

Table 4
The separation energies between each pMDI component and each API material.

pMDI component	Product 1			Product 2		
	Salbutamol sulphate	Mometasone furoate	Salmon calcitonin	Salbutamol sulphate	Mometasone furoate	Salmon calcitonin
	Separation energy ($\times 10^{-18}$ J) (mean; $n = 3 \pm$ S.D.)					
Metering chamber	4.75 (0.7)	5.04 (0.3)	6.03 (1.0)	7.11 (1.0)	8.46 (1.3)	7.95 (0.3)
Valve seal	9.46 (1.2)	6.23 (1.2)	8.45 (0.8)	6.44 (1.4)	7.63 (0.4)	7.33 (0.7)
Outer casing	7.38 (1.4)	6.83 (0.1)	7.45 (0.4)	8.43 (1.7)	12.46 (1.5)	8.64 (1.4)
Valve stem	11.47 (1.8)	14.04 (1.9)	9.77 (0.5)	6.49 (1.4)	6.8 (1.5)	6.56 (0.4)
Valve spring	80.8 (4.7)	30.73 (3.7)	63.22 (5.9)	59.34 (2.9)	37.59 (4.1)	39.52 (1.9)

the area under force–distance curves produced while measuring each API–pMDI interaction. The results are shown in Table 4. From this table, it can be observed that for each of the three API materials, the separation energy from the metering chamber and the valve outer casing is consistently higher for Prod-2 than Prod-1. The opposite is observed when considering the API separation energy from the valve stem. Also, the valve spring from Prod-1 exhibits significantly higher separation energies from salbutamol sulphate and salmon calcitonin, than mometasone furoate. Meanwhile, the mometasone furoate–valve spring interaction from both Prod-1 and Prod-2 is far more comparable.

4.6. Comparisons between thermodynamic work of adhesion and separation energy measurements

The directly proportional relationship between thermodynamic work of adhesion and the force of adhesion (demonstrated in Eqs. (2) and (3)) suggests that it should be possible to correlate the theoretical work of adhesion between interacting surfaces with AFM adhesion interaction measurements (Traini et al., 2005; Traini et al., 2006). Separation energy is calculated by integrating the area under a force–distance curve. By doing this, we are determining the work required to overcome the adhesive forces between two bodies, in order to separate them from contact to infinity. Since work of adhesion is defined as the work required to separate two bodies from contact to infinity (Podczeck, 1998), work of adhesion and separation energy should in theory, be comparable. Thus, for each particulate API, separation energy was correlated with (a) the surface energy of each pMDI valve component, calculated by contact angle measurements (CA_LW), (b) the theoretical work of adhesion (G_{132}^{LW}; calculated from the dispersive component only), (c) the theoretical work of adhesion calculated using the polar component only (G_{132}^{AB}), and finally (d) the total theoretical work of adhesion (G_{132}^{TOT}; calculated from both the dispersive and polar components of surface energy). The results (expressed as R^2 values) for salbutamol sulphate, mometasone furoate and salmon calcitonin are summarised in Table 5.

For both Prod-1 pMDI valve components, the linear relationship between separation energies and CA_LW is not strong (Prod-1; R^2 between 0.59 and 0.67). A weaker correlation between separation energies and CA_LW is observed for Prod-2 (R^2 between 0.19 and 0.23). Poorer correlations exists between separation energy and ΔG_{132}^{LW}, for both Prod-1 (R^2 between 0.02 and 0.12) and Prod-2 pMDI valve components (R^2 between 0.02 and 0.08). However, for both Prod-1 and Prod-2 pMDI valve components, there is a stronger correlation in the linear relationship between separation energies and ΔG_{132}^{AB}. The correlations for Prod-1 valve components resulted in R^2 values between 0.68 and 0.79, while for Prod-2 a significant correlation exists, with R^2 values between 0.92 and 0.94. Moreover, strong linear relationships for both Prod-1 and Prod-2 components were observed when correlating the separation energies with ΔG_{132}^{TOT}, calculated from the dispersive and polar components of surface energy (Prod-1; R^2 between 0.86 and 0.92 and for Prod-2; R^2 between 0.82 and 0.96) (Table 5).

Similar findings have been observed in other studies, where the rank order of salbutamol adhesion to various surfaces, was identical to the theoretical values determined using both dispersive and polar contributions of surface energy (Traini et al., 2006). These results underline the importance of the polar contribution of theoretical surface energy results determined by contact angle measurements, when comparing them to experimental values. Furthermore, when correlating the theoretical work of adhesion and separation energies for each pMDI valve component from Prod-2, the strongest correlation was observed when comparing the separation energy values to the theoretical work of adhesion values calculated for the polar component of surface energy alone. Thus it could be concluded that the polar surface constituents of the polymeric material used by Prod-2 has a much greater dominating influence on their adhesive interactions than that used in Prod-1. This observation was consistent for the interactions of all three API materials, demonstrating that the chemical composition of the polymer used for pMDI valve components affects the interaction with APIs.

For both Prod-1 and Prod-2 it is of interest to note the differences between the separation energies and the functional groups present on both the metering chamber and the valve outer casing. For example, there is a slight relationship between higher energies of separation and an increase in the content of surface hydroxyl (C—OH) and carboxyl (O=C—OH) groups as determined by XPS (Fig. 4). The polymeric material used for the metering chamber and valve outer casing in Prod-1 has a lower level of surface hydroxyl and carboxyl groups which corresponds with lower energies of separation for the API particulate materials. Conversely, the polymeric material used for the metering chamber and valve outer casing in Prod-2 has a higher level of surface hydroxyl and carboxyl groups with higher separation energies for the APIs. The valve stem from Prod-1 was found to have a high level of surface hydroxyl and carboxyl groups with subsequently larger API adhesive forces. Sim-

Table 5
The correlation between ΔG_{132} and separation energy for each API–pMDI component interaction (expressed as R^2 values).

Separation energy vs. . .	Salbutamol sulphate				Mometasone furoate				Salmon calcitonin			
	CA_LW	G_{132}^{LW}	G_{132}^{AB}	G_{132}^{TOT}	CA_LW	G_{132}^{LW}	G_{132}^{AB}	G_{132}^{TOT}	CA_LW	G_{132}^{LW}	G_{132}^{AB}	G_{132}^{TOT}
	Surface energy and theoretical work of adhesion values – separation energy correlations; R^2 values											
Product 1	0.62	0.02	0.76	0.90	0.67	0.04	0.79	0.92	0.59	0.12	0.68	0.86
Product 2	0.23	0.02	0.94	0.92	0.19	0.08	0.92	0.82	0.21	0.03	0.94	0.96

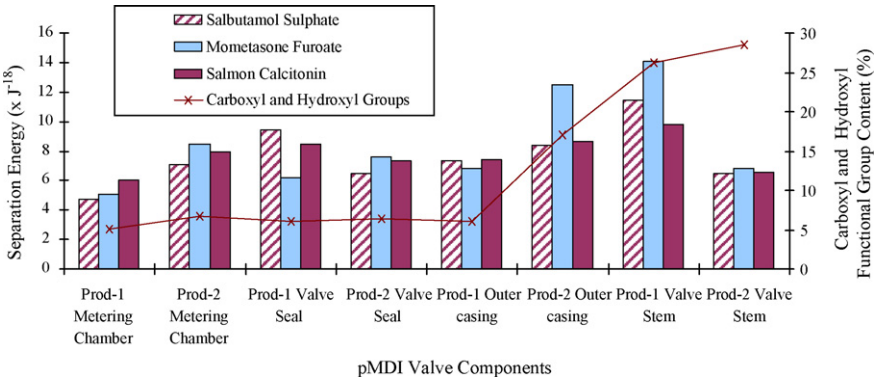

Fig. 4. The relationship between the pMDI component and API separation energy versus the carboxyl and hydroxyl group content of each component.

ilar levels of surface hydroxyl and carboxyl groups were found in each of the valve seals corresponding to similar separation energy values observed between the APIs and the seals from each product. Having said this, the Prod-2 valve stem exhibited lower separation energies, despite containing the highest level of surface carboxyl and hydroxyl groups. Therefore, one can assume that these functional groups are not a dominant factor in the adhesive interactions between the APIs and the valve components used in this study.

These observations are consistent for all the APIs chosen. Having said this, the separation energies and total theoretical work of adhesion values for salbutamol sulphate and calcitonin are approximately the same as each other, while consistently greater than those of mometasone furoate (Tables 3a, 3b and 4). When we consider the surface energy values for these APIs (Fig. 3a) we can see that although the total surface energy values are similar, the γ^+ polar component values are considerably greater for salbutamol sulphate and salmon calcitonin, compared to mometasone furoate. In fact, since both their γ^+ and γ^- component are greater than 1 mJ m^{-2}, they are considered 'bipolar' by definition, whereas mometasone furoate is 'monopolar' (van Oss et al., 1987). Meanwhile, the ΔG_{132} values for both Prod-1 and Prod-2 show higher ΔG_{132} interactions with salbutamol sulphate and salmon calcitonin, compared to mometasone furoate (Tables 3a and 3b). From these tables, a far greater polar surface energy component of the ΔG_{132} values is observed for both salbutamol sulphate and salmon calcitonin when compared to mometasone furoate. Thus, one could suggest that the γ^+ polar component plays an important role in modifying the adhesive interactions between these APIs and the valve components used in this study. The bipolar nature of salbutamol sulphate and salmon calcitonin means that there are electron-donor and electron-acceptor sites at their surfaces, allowing them to interact with both Lewis acids and Lewis bases, and hence explaining their generally greater adhesive interactions when compared to mometasone furoate. Similar observations have been noted in a previous study exploring the adhesive relationships between APIs and bulking excipients in pMDI systems (James et al., 2008). Subsequently, the same principles can clearly be applied to the pMDI components from each manufacturer. For example, the valve springs have bipolar surfaces and correspondingly show the greatest ΔG_{132} interactions to each API. These findings suggest that the bipolar surface energetic nature of not only the API to be used, but also the materials to be employed in the device system, must be considered during the development of an effective and efficient pMDI system.

Variance in contact angles can be a problem when taking measurements on compacted solid surfaces such as those used in this experiment. For instance, both salbutamol sulphate and salmon calcitonin are considerably water-soluble (James et al., 2008) and therefore compacts of these APIs would be penetrated by water droplets during contact angle measurements. This could potentially provide variance in the contact angles measured from these APIs. However, due to the rapid intervals of data recording using the DSA 100M optical Contact Angle meter, it was still possible to gain accurate reproducible contact angle measurements from these samples. Furthermore, all of the contact angles in this study were determined via geometric constructions of each angle on photomicrographs; the method of choice for such samples (Buckton, 1995). Moreover, the calculated surface energy results for salbutamol sulphate are almost identical to those determined elsewhere (Traini et al., 2006). Therefore, it is believed that the determined contact angle results used for this study are accurate.

The van Oss–Chaudhury–Good (vOCG) (van Oss et al., 1988) model used in this study for determining surface energy components via contact angle measurements, is widely accepted and utilised. However, since its inception there have been a number of critiques regarding the method, most of which focus on the choice of liquid probes used during contact angle experiments. Janczuk et al. (1999) performed a study where the surface energy components of various probe liquids were assessed by 'reverse calculations' using polymer surfaces with known surface energy components. Their study found variations in the calculated γ^{LW} values of ethylene glycol, as well as the γ^- and/or γ^+ values of water and diiodomethane. A similar study was performed by Greiveldinger and Shanahan (1999) who also concluded that there is a 'basic-bias' in the measured surface energy of samples, primarily due to the assumption that water is equally Lewis-acidic as it is Lewis-basic. Volpe and Siboni (1997) suggested that more acid solvents should be used as liquid probes in order to diminish any 'basic-bias' in the determined surface energy values of the solid sample. Upon evaluating the vOCG model further, Granqvist et al. (2007) made the same observation regarding 'basic-bias'. Additionally they made a number of conclusions, most notably that the surface tension of the liquids has to be of the same magnitude as the surface energies of the solids in order to provide accurate results. However, one of drawback of these studies is that polymer surfaces generally have a low surface energy with a small acid–base component (Fowkes, 1983). Therefore, some of the findings may not be fully applicable to say, powder samples and other materials of higher surface energy. Nevertheless they do highlight the complex issues which need to be considered in order to accurately determine the surface energy of solid samples.

5. Conclusions

The adhesive interactions between three API materials and pMDI valve components from two different commercially available

products has been characterised using various techniques. Surface roughness was not a significant factor in the adhesive interactions between each API and the pMDI component from either manufacturer. For the valve components of Prod-1, a strong relationship exists when correlating the separation energies to the total theoretical work of adhesion. For the pMDI valve components from Prod-2, the polar component of surface energy yielded the strongest correlation with separation energy. The results generally suggest that for each API–pMDI interaction, the polar component of surface energy has the greatest influence on each adhesive event observed within this experiment (this is particularly dominant when considering the pMDI valve components from Prod-2). The bipolar surface energetics of salbutamol sulphate and salmon calcitonin, as well as certain pMDI components, was deemed responsible for the increased adhesive interactions observed with these materials. This study highlights that different materials can have different effects on the adhesive interactions with particulate APIs. One can conclude that more consideration should be given to determining the surface polar energetics of pMDI components and API particulates in order to minimise API adhesion, and thus produce more effective and efficient pMDI systems.

Acknowledgments

JJ would like to acknowledge the efforts of Prof. Xinyong Chen for his advice and support throughout this study. Also, we thank Mr Michael Taylor for his assistance with the contact angle measurements, and Ms Emily Smith for her assistance with the XPS analysis. Finally, we thank 3M Drug Delivery Ltd. and the EPSRC for the funding of a studentship for JJ.

References

Ashayer, R., Luckham, P.F., Manimaaran, S., Rogueda, P., 2004. Investigation of the molecular interactions in a pMDI formulation by atomic force microscopy. Eur. J. Pharm. Sci. 21, 533–543.

Buckton, G., 1995. Interfacial Phenomena in Drug Delivery and Targeting. Harwood Academic, Switzerland.

Buckton, G., Darcy, P., McCarthy, D., 1995. The extent of errors associated with contact angles. 3. The influence of surface-roughness effects on angles measured using a Wilhelmy plate technique for powders. Colloids Surf. A: Physicochem. Eng. Aspects 95, 27–35.

Chibowski, E., Bolivar, M., González-Caballero, F., 1992. Studies on the surface free energy components of nitrofurantoin. J. Colloid Interface Sci. 154, 400–410.

Davies, M., Brindley, A., Chen, X.Y., Marlow, M., Doughty, S.W., Shrubb, I., Roberts, C.J., 2005. Characterization of drug particle surface energetics and Young's modulus by atomic force microscopy and inverse gas chromatography. Pharm. Res. 22, 1158–1166.

Derjaguin, B., Landau, L., 1941. Theory of the stability of strongly charged lyophobic sols and of the adhesion of strongly charged-particles in solutions of electrolytes. Acta Physicochim. U.S.S.R. 14, 663–692.

Derjaguin, B.V., Muller, V.M., Toporov, Y.P., 1975. Effect of contact deformations on the adhesion of particles. J. Colloid Interface Sci. 53, 314–326.

Eve, J.K., Patel, N., Luk, S.Y., Ebbens, S.J., Roberts, C.J., 2002. A study of single drug particle adhesion interactions using atomic force microscopy. Int. J. Pharm. 238, 17–27.

Fowkes, F.M., 1963. Additivity of intermolecular forces at interfaces. 1. Determination of contribution to surface and interfacial tensions of dispersion forces in various liquids. J. Phys. Chem. 67, 2538–2541.

Fowkes, F.M., 1983. In: Mittal, K.L. (Ed.), Physiochemical Aspects of Polymer Surfaces, vol. 2. Plenum, New York, pp. 583–603.

Gibson, C.T., Weeks, B.L., Abell, C., Rayment, T., Myhra, S., 2003. Calibration of AFM cantilever spring constants. Ultramicroscopy 97, 113–118.

Good, R.J., Girifalco, L.A., 1960. A theory for estimation of surface and interfacial energies. 3. Estimation of surface energies of solids from contact angle data. J. Phys. Chem. 64, 561–565.

Good, R.J., 1993. Contact-angle, wetting, and adhesion—a critical-review (vol. 6, pp. 1269–1302, 1992). J. Adhesion Sci. Technol. 7, 1015–11015.

Granqvist, B., Järn, M., Rosenholm, J.B., 2007. Critical evaluation of the surface energy components of solids. Colloids Surf. A: Physicochem. Eng. Aspects 296, 248–263.

Greiveldinger, M., Shanahan, M.E.R., 1999. A critique of the mathematical coherence of acid/base interfacial free energy theory. J. Colloid Interface Sci. 215, 170–178.

Hooton, J.C., German, C.S., Allen, S., Davies, M.C., Roberts, C.J., Tendler, S.J.B., Williams, P.M., 2004. An atomic force microscopy study of the effect of nanoscale contact geometry and surface chemistry on the adhesion of pharmaceutical particles. Pharm. Res. 21, 953–961.

James, J., Davies, M.C., Bains, B., Toon, R.C., Jinks, P., Roberts, C.J., 2007. The use of AFM to assess macromolecule suspension formulations for metered dose inhalers. J. Pharm. Pharmacol. 59, A45–A145.

James, J., Crean, B., Davies, M., Toon, R., Jinks, P., Roberts, C.J., 2008. The surface characterisation and comparison of two potential sub-micron, sugar bulking excipients for use in low-dose, suspension formulations in metered dose inhalers. Int. J. Pharm. 361, 209–221.

Janczuk, B., Bialopiotrowicz, T., Zdziennicka, A., 1999. Some remarks on the components of the liquid surface free energy. J. Colloid Interface Sci. 211, 96–103.

Johnson, K.L., Kendall, K., Roberts, A.D., 1971. Surface energy and contact of elastic solids. Proc. R. Soc. Lond. Ser. A: Math. Phys. Sci. 324, 301–313.

Katainen, J., Paajanen, M., Ahtola, E., Pore, V., Lahtinen, J., 2006. Adhesion as an interplay between particle size and surface roughness. J. Colloid Interface Sci. 304, 524–529.

Kwok, D.Y., Lam, C.N.C., Li, A., Leung, A., Wu, R., Mok, E., Neumann, A.W., 1998. Measuring and interpreting contact angles: a complex issue. Colloids Surf. A: Physicochem. Eng. Aspects 142, 219–235.

Podczeck, F., 1998. Particle–Particle Adhesion in Pharmaceutical Powder Handling. Imperial College Press.

Price, R., Young, P.M., Edge, S., Staniforth, J.N., 2002. The influence of relative humidity on particulate interactions in carrier-based dry powder inhaler formulations. Int. J. Pharm. 246, 47–59.

Pugh, R.J., Matsunaga, T., Fowkes, F.M., 1983. The dispersibility and stability of carbon-black in media of low dielectric-constant.1. Electrostatic and steric contributions to colloidal stability. Colloids Surf. 7, 183–207.

Smyth, H.D.C., 2003. The influence of formulation variables on the performance of alternative propellant-driven metered dose inhalers. Adv. Drug Deliv. Rev. 55, 807–828.

Traini, D., Rogueda, P., Young, P., Price, R., 2005. Surface energy and interparticulate forces correlations in model pMDI formulations. Pharm. Res. 22, 816–825.

Traini, D., Young, P.M., Rogueda, P., Price, R., 2006. The use of AFM and surface energy measurements to investigate drug-canister material interactions in a model pressurized metered dose inhaler formulation. Aerosol Sci. Technol. 40, 227–236.

van Oss, C.J., Chaudhury, M.K., Good, R.J., 1987. Monopolar surfaces. Adv. Colloid Interface Sci. 28, 35–64.

van Oss, C.J., Chaudhury, M.K., Good, R.J., 1988. Interfacial Lifshitz van der Waals and polar interactions in macroscopic systems. Chem. Rev. 88, 927–941.

van Oss, C.J., 1993. Acid–base interfacial interactions in aqueous media. Colloids Surf. A: Physicochem. Eng. Aspects 78, 1–10.

van Oss, C.J., 1994. Interfacial Forces in Aqueous Media. Marcel Dekker Inc., New York.

van Oss, C.J., Busscher, I.H.J., 1996. In: Spelt, A.W., Neumann, J.K. (Eds.), Applied Surface Thermodynamics. Marcel Dekker, Inc., 646 pp. ISBN 0-8247-9096-0, Colloids Surf. B: Biointerfaces. 9, 121.

Vervaet, C., Byron, P.R., 1999. Drug–surfactant–propellant interactions in HFA-formulations. Int. J. Pharm. 186, 13–30.

Verwey, E.J.W., Overbeek, J.T.G., 1948. Theory of the Stability of Lyophobic Colloids. Elsevier Science Publishers, Amsterdam.

Volpe, C.D., Siboni, S., 1997. Some reflections on acid–base solid surface free energy theories. J. Colloid Interface Sci. 195, 121–136.

Young, P.M., Price, R., Lewis, D., Edge, S., Traini, D., 2003. Under pressure: predicting pressurized metered dose inhaler interactions using the atomic force microscope. J. Colloid Interface Sci. 262, 298–302.

Young, P.M., Price, R., Tobyn, M.J., Buttrum, M., Dey, F., 2004. The influence of relative humidity on the cohesion properties of micronized drugs used in inhalation therapy. J. Pharm. Sci. 93, 753–761.